Bulgarian Academy of Sciences. Space Research and Technology Institute.
Aerospace Research in Bulgaria. 34, 2022, Sofia

WITHIN-FIELD MAPPING OF WINTER WHEAT BIOPHYSICAL VARIABLES USING MULTISPECTRAL IMAGES FROM UAV

Georgi Jelev, Petar Dimitrov, Eugenia Roumenina

Space Research and Technology Institute – Bulgarian Academy of Sciences
e-mail: g_jelev@abv.bg, petarkirilov@mail.bg, roumenina@space.bas.bg

Keywords: *Winter Wheat, LAI, fAPAR, fCover, UAV, Multispectral Camera*

Abstract

The paper presents the results from a study aiming to map the dynamic of biophysical variables of winter wheat crops in different phenological growth stages (PGSs) using multispectral camera data acquired by Unmanned Aerial Vehicle (UAV). The studied biophysical variables are Leaf Area Index (LAI), fraction of Absorbed Photosynthetically Active Radiation (fAPAR) and fraction of vegetation cover (fCover). During agricultural year 2016/2017, 4 field campaigns (FCs) were carried out in 6 farmer-managed fields sown with two winter wheat varieties. During the FCs, 8 UAV flight missions were accomplished. Linear and exponential regression models were designed and evaluated to derive predictive equations for the biophysical variables of the crops based on a set of vegetation indices (VIs). The best predictor for all biophysical variables was OSAVI (RMSE was 0.90 m2/ m2, 0.07 and 0.08 for LAI, fAPAR, and fCover respectively). The chosen models were used to compose maps of LAI, fAPAR, and fCover of the studied fields. The maps correspond well with the spatial distribution of the values of the respective biophysical variables measured during the respective field campaign.

Introduction

Leaf Area Index (LAI), fraction of Absorbed Photosynthetically Active Radiation (fAPAR), and fraction of vegetation Cover (fCover) are biophysical variables of the vegetation cover which are among the major indicators of its status. To evaluate their spatial change, the products LAI, fAPAR, and fCover are formed, using multispectral aerial and satellite data [1 –3]. These products are validated by ground-based measurements of the same parameters on test fields located in various parts of the world. On the territory of Bulgaria, the LAI and FAPAR products from the MERIS satellite sensor were tested on winter wheat fields located in north-east Bulgaria [4]. The new satellite mission Sentinel 2 of the European Space Agency features good spectral, spatial, and temporal resolution [5]. The data from it are already used in precision agriculture, but there are still some limitations related mostly with the days with cloud cover during the image-taking. For this reason,

sometimes the farmers cannot obtain information about their fields for weeks on end. Quite often, when a certain problem arises, the farmers would wish to obtain immediately information about its progress, so as to be able to take informed decision.

The technologies for remote determination of the crops' status using unmanned aerial vehicle (UAV) are increasingly used in precision agriculture [6]. Scientists develop and evaluate different models for timely deriving of information about the dynamics of the agronomic parameters of agricultural crops during major phenological phases from images obtained by UAV cameras [7 –12]. The studies were carried out on one or several adjacent experimental fields of similar small size which are not managed by farmers.

This study was carried out on fields of various sizes, managed by farmers carrying out their agrotechnical activities. Its main objective is within-field mapping of the change of LAI, fAPAR, and fCover of winter wheat crops during different phenological growth stages using data from UAV-borne multispectral camera.

Study area and materials

Study fields

This study was carried out on 6 farmer-managed fields or Units (Us) sown with winter wheat (*Triticum aestivum L.*). They are located on the territory of Zlatia test site, Municipality of Knezha, Pleven region, Bulgaria, Fig. 1, which is part of the north-west planning district of Bulgaria. The Units were spatially grouped in two areas and were managed by two different farmers – U1, U2, and U3 were located on the land of the town of Knezha, and U4, U5, and U6 – on the land of the village of Enitsa. The units feature different area: U1 – 150 ha, U2 – 86 ha, U3 – 10 ha, U4 – 48 ha, U5 – 78 ha, and U6 – 7 ha. Units 1 to 3 were sown with *Anapurna* variety while units 4 to 6 were sown with *Enola* variety. The altitude varies between 80 and 190 m a.s.l. The winter wheat crops were grown on three types of soils [13]. Epicalcic Chernozems Siltic, Endocalcic Chernozem Pachic Siltic (Units 1, 2, and 3), and Haplic Cambisol Eutric Siltic (Units 4, 5, and 6). These are among the most widespread soils in north-west Bulgaria and they are suitable for growing of winter wheat.

Data acquisition and processing

In the study, we used data from field measurements and observations and imagery obtained from Parrot Sequoia UAV multispectral camera, as well as data from the two farmers managing the fields. The data were obtained as a result of the implementation of the TS2AgroBG Project.

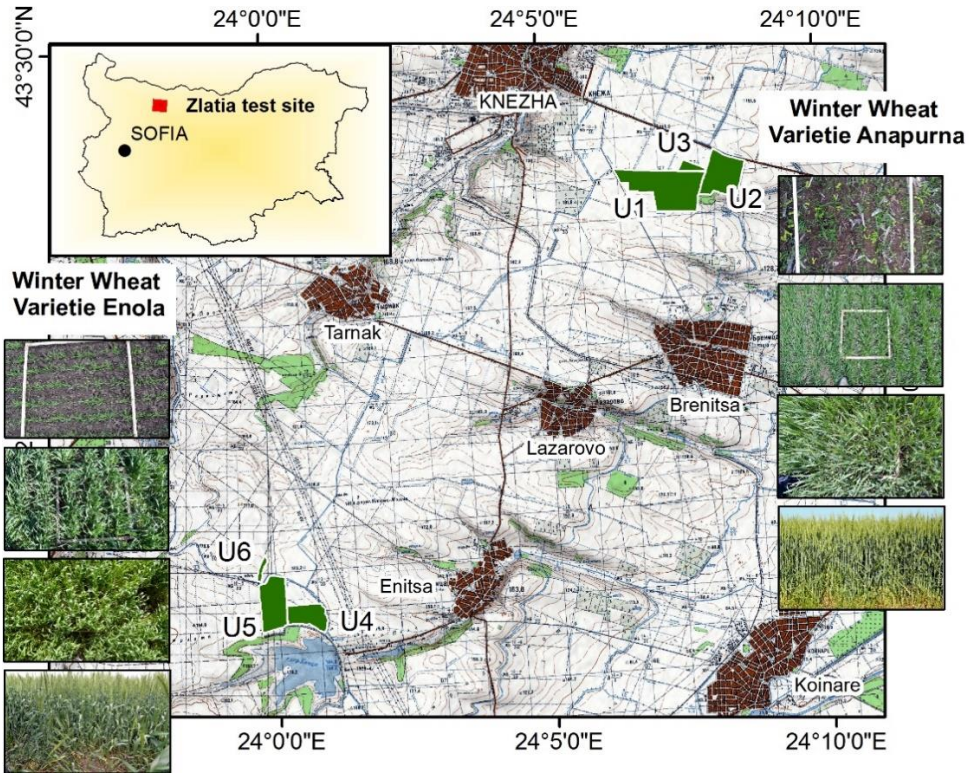

Fig. 1. Location of the Units (U1, U2, U3, U4, U5 and U6) on which the study was carried out in the Zlatia test site, Bulgaria. (Base map source: http://web.uni-plovdiv.bg/vedrin)

Field data

During agricultural year 2016/2017, 4 field campaigns (FCs) were carried out, aiming to collect data about the studied units. They were carried out during 4 major phenological growth stages (PGSs) of the crops, as follows: Tiller production before wintering – FC 1 (07–11.11.2016), Tiller production after wintering – FC 2 (20–24.03.2017), Stem elongation – FC 3 (24–28.04.2017), and Anthesis – FC 4 (15–19.05.2017). To determine the PGS, Zadoks decimal code [14] was used.

The predecessors on the observed Units were sunflower (U1, U2, U3) and maize (U4, U5, U6) which are suitable for growing of winter wheat. On all Units, pre-sowing preparation was carried out and, during sowing, the soil was fertilized with Diammonia phosphate (DAP) – 250 kg/ha in U1, U2, and U3 and 260 kg/ha in U4, U5, and U6. The winter wheat was sown on 03.10.2016 and 09.10.2016, within the optimal terms for its growth in this region of Bulgaria, but for U6 where it was sown later, on 25.10.2016. Units 1, 2, and 3 were sown with 500 seeds per m2, Units 4 and 5 – with 550 seeds per m2, and U6 – with 580 seeds per m2.

During the restoration of winter wheat vegetation after wintering (05.03.2017 and 26.02.2017), spring fertilization with *Urea* was carried out with 180 kg/ha (U1, U2, U3) and 250 kg/ha (U4, U5, U6). There was significant difference in the type of spring fertilization of wheat crops carried out on 25.03.2017. The crops in Units 1, 2, 3 were fertilized with *Ammonium nitrate* (150 kg/ha). On the wheat in Units 4, 5 and 6, foliar fertilization was applied during PGS Tiller production.

On the territory of the studied Units, a total of 30 (Fig, 1) elementary sampling units (ESUs) sized 20×20 m were outlined. Three elementary sub-sampling units sized 1 m^2 were determined within each ESU to perform phenological observations and measurements using the instrument AccuPAR PAR/LAI Ceptometer LP-80. The data from these measurements were averaged for each ESU and were used to determine LAI (m2 m-2), fAPAR and fCover [15]. The obtained data are summarized on Table 1 at Unit level for the units sown with *Anapurna* and *Enola* variety. The distribution of the values of the ground-measured biophysical crop variables for Unit 6 is provided separately because of the differences in the phenological development due to its later sowing, as compared to Units 4 and 5.

Table 1. Descriptive statistics for the ground-measured biophysical crop variables recorded during the 4 carried out field campaigns

Range, Mean and Std. dev.	**Code Unit**	**Phenological growth stages**	**LAI**	**fAPAR**	**fCover**
Range	U1, U2, U3	Z20	0.08-0.41	0.13-0.34	0.03-0.13
	U4, U5	Z20	0.04-0.22	0.12-0.24	0.02-0.07
	U6	Z00	0	0	0
Mean	U1, U2, U3	Z20	0.19	0.20	0.06
	U4, U5	Z20	0.09	0.15	0.04
	U6	Z00	0	0	0
Std. dev.	U1, U2, U3	Z20	0.09	0.06	0.03
	U4, U5	Z20	0.06	0.04	0.02
	U6	Z00	0	0	0
Range	U1, U2, U3	Z21 to 26	0.57-1.54	0.38-0.63	0.23-0.47
	U4, U5	Z21 to 26	1.04-2.62	0.49-0.79	0.35-0.65
	U6	Z20 to 24	0.14-0.35	0.16-0.25	0.06-0.14
Mean	U1, U2, U3	Z21 to 26	0,94	0,48	0,33
	U4, U5	Z21 to 26	1,86	0.68	0.53
	U6	Z20 to 24	0.25	0.21	0.10

Std. dev.	U1, U2, U3	Z21 to 26	0.29	0.07	0.07
	U4, U5	Z21 to 26	0.43	0.09	0.08
	U6	Z20 to 24	0.10	0.04	0.04
Range	U1, U2, U3	Z31 to Z33	2.27-5.30	0.70-0.92	0.64-0.91
	U4, U5	Z31 to Z34	3.36-7.88	0.77-0.95	0.74-0.97
	U6	Z31 to Z33	2.21-2.81	0.68-0.72	0.59-0.66
Mean	U1, U2, U3	Z31 to Z33	3,45	0,83	0,78
	U4, U5	Z31 to Z34	6,19	0.91	0.93
	U6	Z31 to Z33	2,46	0.70	0.62
Std. dev.	U1, U2, U3	Z31 to Z33	0.81	0.06	0.08
	U4, U5	Z31 to Z34	1,23	0.05	0.07
	U6	Z31 to Z33	0.31	0.02	0.04
Range	U1, U2, U3	Z65	2.43-5.86	0.72-0.92	0.65-0.94
	U4, U5	Z65 to 69	3.65-7.09	0.85-0.94	0.81-0.95
	U6	Z65 to 69	3.45-3.73	0.83-0.88	0.80-0.87
Mean	U1, U2, U3	Z65	3,81	0,84	0,82
	U4, U5	Z65 to 69	5,03	0.91	0.92
	U6	Z65 to 69	3,59	0.86	0.84
Std. dev.	U1, U2, U3	Z65	0.99	0.06	0.09
	U4, U5	Z65 to 69	1,11	0.02	0.04
	U6	Z65 to 69	0.14	0.03	0.03

UAV System and Flight Missions

Here During each field campaign, 2 UAV missions were carried out, Table 2, using the *Specialized Unmanned Aerial Vehicle (SUAV) senseFly eBee Ag* including drone, *Parrot Sequoia* multispectral camera, Table 3, plus a sunshine (light) sensor [16], navigation, and image processing software. Before each UAV mission, a flight plan was drawn and simulation of the flight was carried out. The products from the imaging were georeferenced using data from the on-board GPS in UTM coordinate system, zone 35, datum World Geodetic System (WGS) 1984. The ultimate generated product was orthophoto mosaic for the studied Units. To georeference the photomosaic with maximal precision, the coordinates of 13 geographical control points (GCPs) were used which were measured by GNSS Leica GS08. The GCPs were determined before the carrying out of the two UAV missions, being marked by fixed clearly discernible white markers sized 25x25 cm2.

All UAV missions were accomplished at flight altitude of 265 m on clear sunny days, during the period between 11:00 a.m. and 02:00 p.m. local time, at wind velocity below 5 m/s.

Table 2. Dates of the carried out UAV flight missions and PGSs of the winter wheat crops in the studied Units

Flight mission/ID	Flight date UAV	Unit (U)	Phenological Growth Stage
Mission 1/M1	07.11.2016	U1 and U3	Tiller production, (Z20)
	11.11.2016	U2	
Mission 2/M2	10.11.2016	U4, U5 and U6	U4, U5 – Tiller production, (Z 20), U6 – Unspr \outed Z00
Mission 3/M3	21.03.2017	U1, U2 and U3	Tiller production: Zadoks 21 to 26
Mission 4/M4	22.03.2017	U4, U5 and U6	Tiller production: U4, U5 – Z21 to Z26, U6 – Z20 to 24
Mission 5/M5	25.04.2017	U1, U2 and U3	Stem elongation: Z31 to Z33
Mission 6/M6	26.04.2017	U4, U5 and U6	Stem elongation: U4, U5 - Z31 to Z34, U6 – Z31 to Z32
Mission 7/M7	15.05.2017	U4, U5 and U6	Anthesis: U4 – Z65, U5 – Z69, U6 – Z65 to 69
Mission 8/M8	18.05.2017	U1, U2 and U3	Anthesis (flowering): Z65

Table 3. Spectral bands for the Parrot Sequoia UAV camera used in the study

Channel name	Green (Bg)	Red (Br)	Red edge (Bre)	Near IR (Bnir)
Central wavelength (nm)	550	660	735	790
Bandwidth (nm)	40	40	10	40
Spatial resolution (m/pixel)	0.20	0.20	0.20	0.20

Methodology

The maps of the crops' biophysical variables in the studied Units were composed in 2 stages. During the first one, regression models for LAI, fAPAR and fCOVER were designed, and during the second one, the relevant maps were composed.

Designing of regression models for LAI, fAPAR, and fCOVER

Methods

We used regression analysis in order to find predictive equations for the biophysical variables based on a set of vegetation indices (VIs), Table 4, and the four spectral bands. Linear and exponential models were developed using one predictor at a time and thus all VIs/bands were evaluated for their predictive capability. The 2016-2017 growing season data were used for model calibration and leave-one out cross validation. ESUs with significant weed coverage were omitted from the dataset.

Table 4. List of spectral vegetation indices used in this study and formulas for their calculation

Vegetation Index	Formulae	Reference
Chlorophyll Index green (CIg)	(NIR / Green) – 1	[17, 18]
Chlorophyll Index red edge (CIre)	(NIR / Red edge) - 1	[17, 18]
Difference Vegetation Index (DVI)	NIR - Red	[19]
Green Infrared Percentage Vegetation Index (GIPVI)	NIR/(NIR + Green)	
Green Normalized Difference Vegetation Index (gNDVI)	(NIR – Green) / (NIR + Green)	[20]
Green Normalized Difference Vegetation Index 1 (gNDVI 1)	(Red edge – Green) / (Red edge + Green)	
Modified Triangular Vegetation Index 2 (MTVI2)	$\frac{1.5*\left[1.2*\left(NIR-Green\right)-2.5*\left(Red-Green\right)\right]}{\sqrt{\left(2*NIR+1\right)^2-\left(6*NIR-5\sqrt{Red}\right)-0.5}}$	[7]
Normalized Difference Vegetation Index (NDVI)	(NIR – Red) / (NIR + Red)	[21]
Normalized Difference Vegetation Index 1 (NDVI 1)	(Red edge – Red) / (Red edge + Red)	
Optimized Soil-Adjusted Vegetation Index (OSAVI)	(1+0.16)*(NIR - Red) / (NIR + Red + 0.16)	[22]
Red edge Normalized Difference Vegetation Index (reNDVI)	(NIR –Red-edge) / (NIR + Red-edge)	[23]
Simple Ratio (SR)	NIR / Red	[19]
Simple Ratio 1 (SR 1)	Red-edge / Red	
Simple Ratio 3 (SR 3)	NIR / Red-edge	[23]
Vegetation Index green (VIg)	(Green – Red) / (Green + Red)	[24]
Wide Dynamic Range Vegetation Index (WDRVI)	(0.3 * NIR – red) / (0.3 * NIR + Red)	[25]

The performance of the models was evaluated based on the Root Mean Square Error (RMSE):

1) $$RMSE = \sqrt{\frac{\sum_i (y_i - \hat{y}_i)^2}{n}},$$

where: y_i is the measured value for the i-th observation and $\hat{y}_i$ is the predicted value for i derived from a model calibrated with all observations except i. Relative RMSE ($RMSE_r$) was calculated as percentage of the mean of the measured values.

Results

Table 5 shows the error statistics of the regression equations derived by each predictor. For each combination of biophysical variable and predictor two models, i.e. linear and exponential, were developed and the one with lower error were selected and considered for the comparison in Table 5. For all biophysical variables the best predictor was OSAVI. The relationships with OSAVI were exponential, Fig. 2. The corresponding regression equations are shown in Table 6.

Table 5. Root mean square errors (RMSE) and relative Root mean square errors (RMSEr) from the leave-one-out cross validation of the regression models. Model type is either linear (lin), or exponential (exp). For each biophysical variable the three lowest RMSE/RMSEr values are shown in bold.

Predictor	LAI			fAPAR			fCover		
	Model type	**RMSE [m^2/m^2]**	**$RMSE_r$ [%]**	**Model type**	**RMSE [-]**	**$RMSE_r$ [%]**	**Model type**	**RMSE [-]**	**$RMSE_r$ [%]**
Green band	lin	2.08	68.8	lin	0.26	38.9	lin	0.31	50.4
Red band	lin	2.19	72.6	lin	0.27	39.7	lin	0.33	52.8
Red edge band	exp	1.22	40.5	lin	0.14	20.2	lin	0.17	27.3
NIR band	exp	**0.96**	**31.7**	lin	0.08	12.0	lin	0.09	14.6
CIg	lin	1.39	46.1	lin	0.13	18.9	lin	0.16	26.7
CIre	lin	1.39	46.0	lin	0.11	16.8	lin	0.13	21.2
DVI	exp	**0.94**	**31.3**	lin	**0.08**	**11.3**	lin	**0.09**	**14.0**
GIPVI	exp	1.40	46.4	exp	0.12	17.1	lin	0.17	27.1
gNDVI	exp	1.40	46.4	exp	0.12	17.1	exp	0.16	25.9
gNDVI1	lin	1.79	59.5	lin	0.19	28.3	lin	0.24	39.7
MTVI2	exp	0.99	32.7	exp	**0.07**	**10.1**	exp	**0.09**	**13.8**
NDVI	exp	1.47	48.7	exp	0.12	17.1	exp	0.15	25.0
NDVI1	exp	1.75	58.2	exp	0.17	25.0	lin	0.22	36.4
OSAVI	exp	**0.93**	**30.8**	exp	**0.07**	**10.0**	exp	**0.08**	**13.1**
reNDVI	lin	1.35	44.7	lin	0.09	13.7	lin	0.11	18.2

SR	lin	1.52	50.4	lin	0.13	19.7	lin	0.17	28.1
SR1	lin	1.80	59.6	lin	0.19	27.4	lin	0.24	38.6
SR3	lin	1.39	46.0	lin	0.11	16.8	lin	0.13	21.2
VIg	lin	1.91	63.2	lin	0.20	29.0	lin	0.25	40.1
WDRVI	exp	1.48	49.1	exp	0.11	16.8	exp	0.16	25.5

Table 6. Regression model selected for the mapping of the biophysical variables

Biophysical variable	Regression equation
LAI	LAI = 0.00193 * exp(OSAVI * 9.31558)
fAPAR	fAPAR = 0.05485 * exp(OSAVI * 3.32069)
fCover	fCover = 0.01119 * exp(OSAVI * 5.20752)

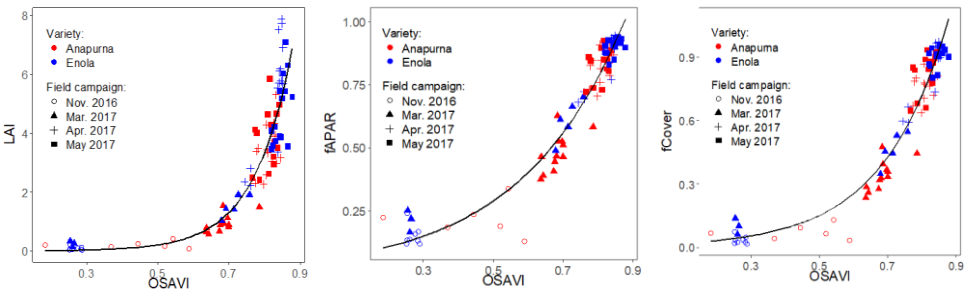

a) b) c)

Fig. 2. Scatter plots of biophysical variables LAI (a), fAPAR (b), and fCover (c) and OSAVI showing the exponential regression fit

Composing of maps of LAI, fAPAR, and fCOVER

In the beginning of this stage, a geodatabase was composed. It included: the boundaries of the studied Units, soil maps, digital elevation model (DEM), the data from the carried out field campaigns, and the images obtained from all UAV flight missions; Crop Calendar containing information about the agrotechnical measures carried out by the farmers, and data about the initial and final dates of occurrence of the major phenological phases of the winter wheat crops for each individual Unit. Input into the geodatabase were also the designed regression models for calculation of the crops' biophysical variables, as well as the results from the processing and analysis of the multispectral UAV images.

The maps of the crops' biophysical variables were composed in the following steps. Initially, the orthophoto mosaic of the multispectral images obtained from each UAV flight mission was cropped along the boundaries of each Unit. Out

of them, the vegetation index OSAVI for each pixel was calculated and a raster image was obtained, on which the respective regression model for LAI, fAPAR and fCOVER was applied successively, Table 6. The raster layer thus calculated was reclassified into 5 classes with previously fixed boundaries. As a result, a raster layer was obtained which was used to draw a separate map for each biophysical parameter, Fig. 3, 4, and 5.

Results and discussion

The crops studied during the observed agricultural year 2016/2017 do not differ significantly in their phenological growth, but for those in Unit 6. In it, due to the later sowing, a delay in the dates of the mass occurrence of PGS *Germination Z 0-1* and *Stem elongation Z 31 to 34* was observed, as compared to the other crops.
Maps of LAI, Fig. 3, were composed, obtained by applying a regression model based on the OSAVI vegetation index, Table 6, on images from *Parrot Sequoia* UAV multispectral camera acquired during the carried out UAV flight missions, Table 2.

On them, the obtained values of LAI and their distribution during PGSs *Tiller production, Stem elongation,* and *Anthesis* comply with the ground-measured ones during the carried out FCs, Fig. 3, Table 1.

On the map of LAI, Fig.3, drawn using images from UAV missions 3 and 4, one can easily distinguish between Units 1, 2, 3, and 6, from one hand, which feature lower LAI vallues (0.15-1.5 m^2/m^2) and Units 4 and 5, from the other hand (LAI between 0.15-3.0 m^2/m^2). This coincides with the ground-measured values of LAI which are within the same limits, Table 1. The same differences are also observed on the maps composed for PGS *Stem elongation* Fig. 3 b, Table 1. The average value of LAI by data obtained from ground-based measurements in U1, U2, and U3 is 3.45 m^2m^{-2}, while in U4 and U5 it is much higher – 6.19 m^2/m^2, being lowest again in U6 – 2.46 m^2/m^2.

The recorded values of LAI on the maps where the crop is in PGS *Anthesis*, Fig. 3c, are identical with those on the maps for PGS *Stem elongation*, Fig. 3b. The only exceptions are U6, the southern part of U1, and the western part of U4 where the values are higher. This is also confirmed by the data from the ground-based measurements, Table 1, but for U4 and U5 where a certain decrease of the average values of LAI by 1.17 m^2/m^2 is observed. This inconsistency of the modeled LAI with ground measurements at PGS Anthesis may be explained with the lower sensitivity (saturation issues) of the exponential model at high LAI values.

The reasons for the established differences in the values of the crops' LAI in U1, U2 and U3 compared to those in U4 and U5 are complex. Probably, they are due not only to the fact that they have been sown with different varieties of winter wheat, but also because they differ in the applied spring fertilization, as described in Section *Field data*. On U4 and U5, in the end of March 2017, foliar feeding of wheat was also carried out. The grain yield is classified in the *feed wheat category* in the

crops of winter wheat variety *Anapurna*, and *normal bread wheat* category for variety *Enola*.

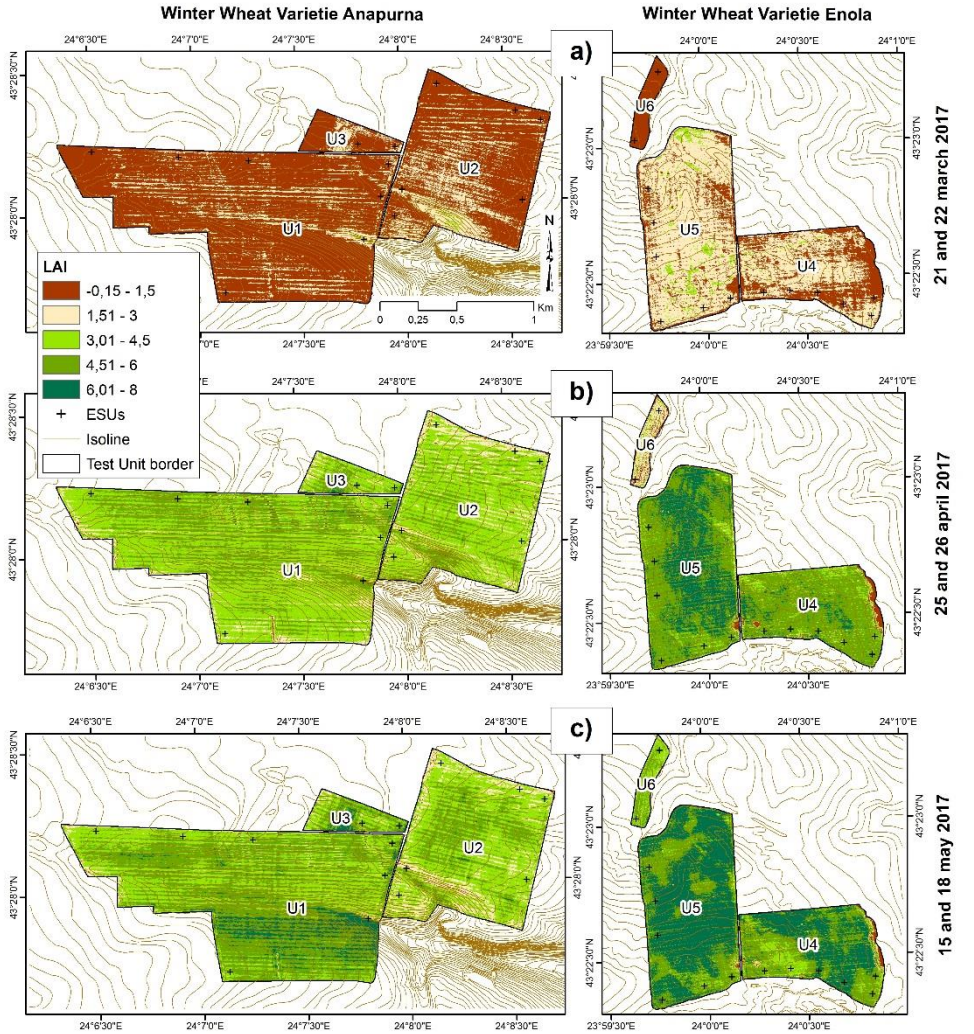

Fig. 3. Maps of LAI of winter wheat crops in the studied Units composed by applying an regression model based on the OSAVI vegetation index on images from Parrot Sequoia UAV multispectral camera obtained from UAV flight missions: a) missions 3 and 4, FGS Tiller production, b) missions 5 and 6, FGS Stem elongation, and c) missions 7 and 8, FGS Anthesis

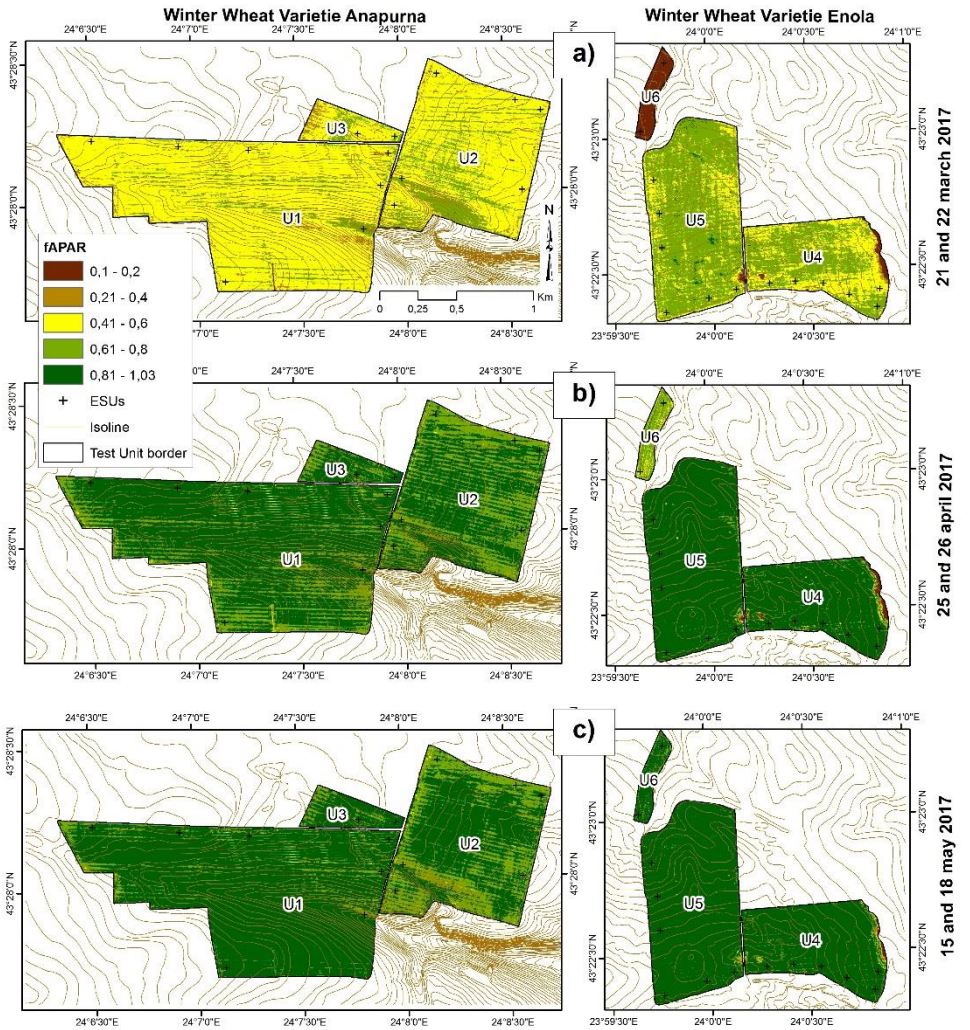

Fig. 4. Maps of fAPAR of winter wheat crops in the studied Units composed by applying an regression model based on the OSAVI vegetation index on images from Parrot Sequoia UAV multispectral camera obtained from UAV flight missions: a) missions 3 and 4, FGS Tiller production, b) missions 5 and 6, FGS Stem elongation, and c) missions 7 and 8, FGS Anthesis

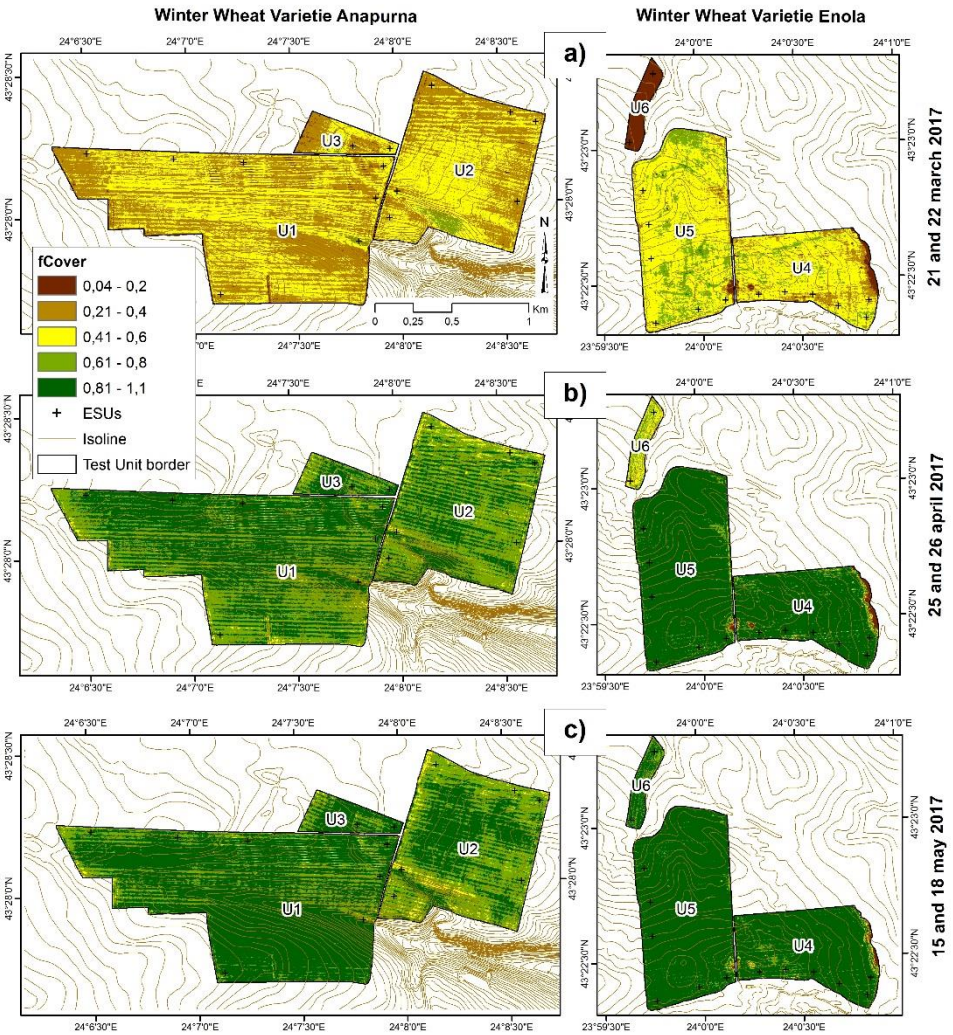

Fig. 5. Maps of fCOVER of winter wheat crops in the studied Units composed by applying an regression model based on the OSAVI vegetation index on images from Parrot Sequoia UAV multispectral camera obtained from UAV flight missions: a) missions 3 and 4, FGS Tiller production, b) missions 5 and 6, FGS Stem elongation, and c) missions 7 and 8, FGS Anthesis

On the drawn maps of the other two biophysical variables it may be seen that the recorded values of fAPAR and fCover on U1–U3 differ from those on U4–U5, Fig. 4 and 5, only in PGS *Tiller production: Zadoks 21 to 26*, Fig. 4a and 5a. In

Unit 6, in PGSs *Tiller production* and *Stem elongation*, the crop features lower values of both variables, Fig. 4a,b and 5 a,b.

Conclusions

The best predictor for all studied biophysical variables, was OSAVI – RMSE, for LAI is 0.90 m^2/ m^2, for fAPAR – 0.07, and for fCover – 0.08.

The composed maps for LAI, fAPAR and fCOVER obtained by applying the respective regression model, based on the vegetation index OSAVI, on images from *Parrot Sequoia* UAV multispectral camera, correspond well with the spatial distribution of the values of the respective parameter, measured during the given field campaign.

Clearly expressed tendencies in the change of LAI values are observed. They increase up to PGS *Stem elongation*, whereas the rate of increase with the winter wheat crops of the *Anapurna* variety is smaller. The change is insignificant between PGSs *Stem elongation* and *Anthesis*.

Acknowledgments

This study was conducted as part of the "Testing Sentinel-2 vegetation indices for the assessment of the state of winter crops in Bulgaria (TS2AgroBg)" project funded by the Government of the Republic of Bulgaria through ESA Contract 4000117474/16/NL/NDe under the Plan for European Cooperating States.

We pay our gratitude also to the farmers Mrs. Nikolai and Tihomir Milovski, Mr. Svetlin Ilchovski, and the agronomist Mrs. Polina Marinska for the provided data and the carried out useful discussions.

References

1. Fang, H., F. Baret, S. Plummer and G. Schaepman-Strub. An overview of global leaf area index (LAI): Methods, products, validation, and applications. Reviews of Geophysics, 2019, 57 (3).
2. Wójtowicz, M., A. Wójtowicz and J. Piekarczyk. Application of remote sensing methods in agriculture. Communications In Biometry and Crop Science. 2016, 11(1), 31–50.
3. Wenjuan, Li, M. Weiss, F. Waldner, et al. A Generic Algorithm to Estimate LAI, FAPAR and FCOVER Variables from SPOT4_HRVIR and Landsat Sensors: Evaluation of the Consistency and Comparison with Ground Measurements. Remote Sensing. 2015, 7 (11), 15494-15516
4. Roumenina, E., P. Dimitrov, L. Filchev and G. Jelev. Validation of MERIS LAI and FAPAR products for winter wheat-sown test fields in North-East Bulgaria. International Journal of Remote Sensing. 2014, 35 (10), 3859-3874.
5. Weiss, M. and F. Baret. S2ToolBox Level 2 products: LAI, FAPAR, FCOVER. INRA. 2016, V1.1, 53.
6. Shanmugapriya, P., S. Rathika, T. Ramesh and P. Janaki. Applications of Remote Sensing in Agriculture - A Review. Int.J.Curr.Microbiol. App. Sci. 2019, 8(1): 2270-2283.

7. Haboudane, D., J. Miller, E. Pattey, et al. Hyper-spectral vegetation indices and novel algorithms for predicting green LAI of crop canopies: modeling and validation in the context of precision agriculture. Remote Sensing of Environment. 2004, 90, 337–352.
8. Sugiura, R., N. Noguchi and K. Ishii. Remote-sensing technology for vegetation monitoring using an unmanned helicopter. Biosyst. Eng. 2005, 90, 369–379.
9. Hunt, E., W. Hively, S. Fujikawa, et al. Acquisition of NIR-green-blue digital photographs from unmanned aircraft for crop monitoring. Remote Sensing. 2010, 2(1), 290–305.
10. Schirrmann, M., A. Giebel, F. Gleiniger, et al.. Dammer. Monitoring Agronomic Parameters of Winter Wheat Crops with Low-Cost UAV Imagery. Remote Sensing. 2016, 8(9), 706.
11. Holman, F., A. Riche, A. Michalski, et al. High Throughput Field Phenotyping of Wheat Plant Height and Growth Rate in Field Plot Trials Using UAV Based Remote Sensing. Remote Sensing. 2016, 8 (12), 1031.
12. Yue, J., H. Feng, X. Jin, et al. A Comparison of Crop Parameters Estimation Using Images from UAV-Mounted Snapshot Hyperspectral Sensor and High-Definition Digital Camera. Remote Sensing. 2018, 10(7), 1138.
13. Kolchakov, V., M. Kercheva, M. Banov, et al. Complex evaluation of winter wheat growing conditions in Northwestern Bulgaria. Proceedings of the 10-th International Soil Congress "Successful Transformation toward Land Degradation Neutrality: Future Perspective", 17-19 June 2019, Ankara, Turkey, 10, 482-487.
14. Zadoks, J., T. Chang and C. Konzak. A decimal code for the growth stages of cereals. Weed Research. 1974, 14, 415-421.
15. Decagon Devices. AccuPAR PAR/LAI Ceptometer, Model LP-80. Operator's Manual Version June 20. 2014, 78.
16. Parrot Sequoia. Available online: https://community.parrot.com/t5/Sequoia/bd-p/Sequoia (accessed on 18.12.2019).
17. Gitelson, A., Y. Gritz and M. Merzlyak. Relationships between leaf chlorophyll content and spectral reflectance and algorithms for non-destructive chlorophyll assessment in higher plant leaves. Journal of Plant Physiology. 2003, 160, 271–282.
18. Gitelson, A., G. Keydan and M. Merzlyak. Three-band model for noninvasive estimation of chlo-rophyll, carotenoids, and anthocyanin contents in higher plant leaves. Geophysical Research Letters. 2006, 33, L11402.
19. Jordan, C. Derivation of leaf-area index from quality of light on the forest floor. Ecology. 1969, 50, 663–666.
20. Gitelson, A., Y. Kaufman and M. Merzlyak. Use of a green channel in remote sensing of global vegetation from EOS-MODIS. Remote Sensing of Environment. 1996, 58, 289–298.
21. Rouse, J., R. Haas, J. Schell and D. Deering. Monitoring vegetation systems in the great plains with ERTS. In: Third ERTS Symposium, NASA SP-351, 1973, vol. 1, NASA, Washington, DC, 309–317.
22. Rondeaux, G., M. Steven and F. Baret. Optimization of soil-adjusted vegetation indices. Remote Sensing of Environment. 1996. 55(2), 95-107.
23. Gitelson, A. and M. Merzlyak. Spectral reflectance changes associated withautumn senescence of Aesculus hippocastanum L. and Acer platanoides L. Leaves. Spectral

features and relation to chloro-phyll estimation. Journal of Plant Physiology. 1994, 143, 286–292.
24. Gitelson, A., Y. Kaufman, R. Stark and D. Rundquist. Novel algorithms for remote estimation of vegeta-tion fraction. Remote Sensing of Environment. 2002, 80, 76–87
25. Gitelson, A. Wide Dynamic Range Vegetation Index for Remote Quantification of Biophysical Charac-teristics of Vegetation. Journal of Plant Physiology. 2004, 161. 165–173

КАРТОГРАФИРАНЕ НА БИОФИЗИЧНИ ПРОМЕНЛИВИ НА ПОСЕВИ ОТ ЗИМНА ПШЕНИЦА С ИЗПОЛЗВАНЕ НА МНОГОКАНАЛНИ ИЗОБРАЖЕНИЯ ОТ БЛА

Г. Желев, П. Димитров, Е. Руменина

Резюме

В статията са представени резултати от проведено изследване с цел картографиране на динамиката на биофизични променливи на посеви от зимна пшеница в различни фенологични фази, чрез използване на данни получени от безпилотен летателен апарат (БЛА) с многоканална камера. Изследваните биофизични променливи са индекс на листната повърхност (LAI), дял на абсорбираната фотосинтетично активна радиация (fAPAR) и дял от повърхността на почвата покрита с растителност (fCover). През селскостопанската година 2016/2017 са проведени 4 полеви кампании (ПК) в 6 полета, стопанисвани от фермери, засети с два сорта зимна пшеница. В рамките на ПК са реализирани 8 полетни мисии с БЛА. Съставени и оценени са линейни и експоненциални регресионни модели за изчисляване на биофизичните променливи на посевите на базата на набор от вегетационни индекси (ВИ). Като най-добър предиктор за всички биофизични променливи е определен OSAVI (RMSE е 0.90 m2/m2, 0.07 и 0.08, съответно за LAI, fAPAR, и fCover). Избраните модели са използвани за съставяне на карти на LAI, fAPAR и fCover на изследваните полета. Картите в значителна степен отговарят на пространственото разпределение на стойностите на съответната биофизична променлива измерени по време на дадената полева кампания.